Calibration of triaxial accelerometers by constant rotation rate in the gravitational field

Michael Gaitan, Jon Geist

National Institute of Standards and Technology, Gaithersburg, MD 20899, USA

A R T I C L E   I N F O

A B S T R A C T

We extend the use of the intrinsic properties calibration method for triaxial accelerometers that we reported previously from discrete angular steps to using a constant rotation rate to produce a time varying sinusoidal excitation in the earth's gravitational field. We show that this extension yields the low frequency calibration response of the device under test. Whereas traditional vibration-based methods using shakers generally exhibit an increased measurement uncertainty with decreased excitation frequency, we show that this approach does not. We report results obtained from a commercial triaxial digital accelerometer from DC up to a 0.5 Hz rotation rate. The maximum rotation rate that we report is limited by our rotation stage; but we expect that the method can be extended to higher rotation rates with an upper limit constrained by what can be tolerated as a maximum centripetal acceleration.

1. Introduction

Microelectromechanical Systems (MEMS)-based triaxial accelerometers and gyroscopes are manufactured in the millions of units each year and are used in a wide range of applications including non-critical uses in smart phones, gaming systems, exercise and health monitors, drones, and in critical uses (where life and limb are at stake) such as in medical devices, automobiles, and military and aerospace systems. The continuing advance of applications and performance metrics of these devices has been a motivation factor for our group's research and development of primary calibration protocols to meet what we view as an emerging need for world-wide equivalence of primary-based calibration of these sensor technologies. One of the methods used by high volume manufacturers for testing and calibration of MEMS-based triaxial inertial accelerometers, and likely the most used, is based on facing each of the three (*x, y, z*) axes of the Device Under Test (DUT) upwards and downwards to the direction of the earth's gravitational field. Following a procedure reported in an application note by Pedley [1] results in at least six measured data points that are used with a Cartesian coordinate system model of the DUT to yield the on-axis and cross axis sensitivities of each of the (X, Y, Z) accelerometers.

The Consultative Committee for Acoustics, Ultrasound and Vibration (CCAUV) [2], has defined methods used to establish the degree of equivalence of accelerometer calibrations that have been adopted and supported by the world's National Measurement Institutes (NMIs).

Central to these methods are key comparisons based on the International Standards Organization's ISO 16063 series of standards on "Methods for the calibration of vibration and shock transducers." An accelerometer key comparison involves the selection of a reference transducer that will be passed to each of the participating NMIs who each follow the agreed upon calibration protocol and report their result to the pilot laboratory. The pilot NMI works collaboratively with the participating NMIs to analyze the results to determine the weighted average of the measurements which is used to establish the degree of equivalence of each participating NMI's measurement. Optimally, the weighted average should agree with the value reported by each NMI to within their reported measurement uncertainties. Disagreements, depending on their nature, may prompt some NMIs to reevaluate their implementation of the measurement protocol and to take corrective action.

The state of the art in acceleration calibrations prior in 2000 was reviewed in detail in [3]. In a summary of world-wide capabilities, 73% of NMI-level laboratories participating in vibration- calibration round robins carried out from 1983 to 1989 produced results deviating from the mean by ≤0.5% at 160 Hz. In similar summaries of Eastern European, European Union, and Asia-Pacific capabilities carried out in 1987–89, 1993–95, and 1996–98, respectively, 60% (63%), 100% (70%), and 100% (67%) produced results deviating from the mean by ≤0.5% (1%) at 160 Hz (10 Hz). The state of the art has improved substantially since then. For instance, in a similar summary of Inter-American capabilities carried out in 2017–2019, 86% (75%) produced

results deviating from the mean by $\leq 0.2\%$ at 160 Hz (10 Hz).

However, there is currently no key comparison directly related to the gravity-based calibration protocol that is used for the majority of accelerometers manufactured every year. The CCAUV recognizes this as a future challenge in their 2019 to 2029 Strategy document [4] and summarizes it in [5] stating that "*Miniaturization technologies for inertial measurement units is driving new applications, significant growth in their production, and needs for primary calibration technologies to support new applications. Compatibility with digital sensor interfaces is also requested; this need is recognized to be a cross-cutting need in AUV as well as other CCs.*" In the same document, the CCAUV also recognized the need for *calibration at ultra-low-frequencies below 0.1 Hz, even to 0.008 Hz and ground motion acceleration/velocity in the frequency range 0.02 Hz to 20 Hz.*

Rectilinear displacement has been used to generate sinusoidal motion for vibration calibrations, a homodyne or heterodyne laser interferometer has been used measure the displacement, and displacement or velocity traceable to the International System of Units (SI) with the resulting acceleration calculated by differentiation. There is a trade-off between frequency range and motion amplitude because the displacement required to produce a given acceleration increases as the square of frequency. As a result, suitable equipment to generate sinusoidal accelerations at low frequencies by rectilinear displacement has been large, expensive, and time consuming. An additional challenge is to implement such vibration-based calibrations for triaxial accelerometers. Umeda et. al. reported on a method to calibrate tri-axial accelerometers using a three-dimensional vibration generator and three laser interferometers [6] from 50 Hz to 500 Hz. D'Emilia et. al. reported on a low-cost rotational reciprocation approach to produce a time varying centripetal acceleration at 0.5 Hz [7] with a repeatability of 0.2%. More recently, a method has been introduced that is based on vibration of a triaxial accelerometer placed on an inclined plane and optimized to reduce the number of measurements needed by mounting the device under test in optimal orientations on the shaker [8,9,10].

Our group recently introduced an intrinsic properties model [11] and calibration protocol similar to what Pedley described in [1] based on orienting the triaxial accelerometer in the earth's gravitational field to determine zero-frequency (DC) sensitivity matrix of tri-axial accelerometers. We later demonstrated that this protocol reproduced the diagonal terms of the sensitivity matrix of the triaxial accelerometer to within $\pm 0.01\%$ and was insensitive to mounting misalignments through $\pm 5°$. The protocol also reproduced the intrinsic sensitivities of the individual accelerometers to this level and the intrinsic angles between the axes of maximum responsivity of the accelerometers to $\pm 0.1°$.

In this report we extend the DC intrinsic-properties calibration protocol to use at a constant rotation rate. This method is optimum for extending low frequency calibrations down to DC because the uncertainties do not increase with decreasing frequency as is the case for vibration-based methods. The method is enabled by wireless communication of the measurement results from the mounting platter of the rotation table during the measurements which is not practical for wired data recording. Subject to the assumption that the rotation-rate is constant and free of nutation or other deviation from pure rotational motion due to instrument distortion, the upper frequency limit of this method is determined by the linear range of the accelerometer. This results in a pure sinusoidal excitation of the accelerometers superimposed on a constant centripetal force where the excitation frequency corresponds to the rotation rate, thereby enabling the characterization of the accelerometer's intrinsic properties as a function of frequency. When used together with the DC approach we show that we can measure the frequency response of the triaxial accelerometer from DC up to the rotation limit set by the calibration equipment.

2. The intrinsic properties model applied to constant rotation

Following the derivation presented in [12], the intrinsic properties of

the triaxial accelerometer device under test (DUT) are defined in terms of accelerometers (U, V, W) depicted in Fig. 1 whose unit vectors $(\hat{u}, \hat{v}, \hat{w})$ point in the direction of maximum sensitivity of each of the (U, V, W) accelerometers, respectively, and having angles between them ($\varphi_{uv}, \varphi_{vw}, \varphi_{wu}$) representing the angles between the (U, V), (V, W), and (W, U) accelerometers, respectively. The (U, V, W) accelerometers are considered to only respond to accelerations that are parallel to their unit vectors and are defined to have sensitives (s_u, s_v, s_w), respectively. The intrinsic properties also include the dc offsets of each of the (U, V, W) accelerometers defined as (O_u, O_v, O_w), respectively, making up a total of nine intrinsic properties to describe the response of the DUT: (s_u, s_v, s_w), ($\varphi_{uv}, \varphi_{vw}, \varphi_{wu}$), and ($O_u, O_v, O_w$).

The DUT is placed onto the platter of a 2-axis rotation stage with its (U, V, W) accelerometers approximately aligned to the stage's (X, Y, Z) Cartesian coordinate system as depicted in Fig. 2, with axes of rotation defined as **axis 1** whose rotation is specified by the angle ϕ and **axis 2** whose rotation is specified by the angle θ.

Under static conditions the response of the accelerometers is specified by [9]:

$$\begin{bmatrix} U(\theta, \phi) \\ V(\theta, \phi) \\ W(\theta, \phi) \end{bmatrix} = g_{loc} \begin{bmatrix} s_{ux} & s_{uy} & s_{uz} \\ s_{vx} & s_{vy} & s_{vz} \\ s_{wx} & s_{wy} & s_{wz} \end{bmatrix} \begin{bmatrix} \sin(\theta)\sin(\phi) \\ \sin(\theta)\cos(\phi) \\ \cos(\theta)\cos(\phi) \end{bmatrix} + \begin{bmatrix} O_u \\ O_v \\ O_w \end{bmatrix}, \qquad (1)$$

where the 3×3 matrix is defined as the sensitivity matrix having main components s_{ux}, s_{vy}, and s_{wz} of the (U, V, W) accelerometers in the directions of the (X, Y, Z) Cartesian coordinate axes, coupled with their cross-axis components which are orthogonal to those main components. The sensitivity matrix will vary as a function of any misalignment of the DUT to the axes of the calibration equipment, but the intrinsic properties have been shown to be invariant to misalignment [12]. The term g_{loc} is the local value for the earth's gravitational acceleration measured or determined at the location of the calibration. In this report we use the value of $9.80101 \pm 3 \times 10^{-5}$ m s^{-2} which we determined using the National Geodetic Survey's Surface Gravity Prediction web-based calculator using the latitude and longitude of the location of the calibration equipment [13].
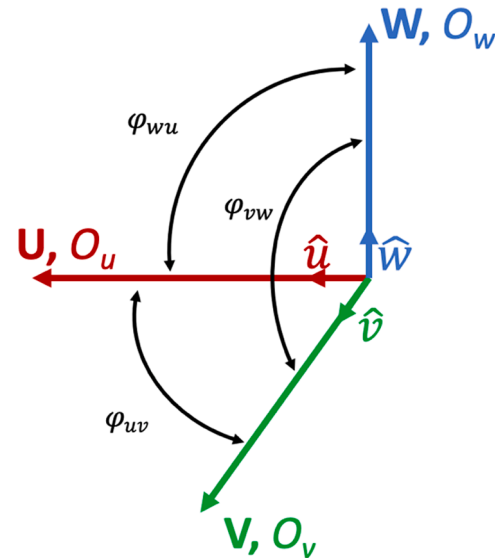

Fig. 1. Drawing of the intrinsic model of a triaxial accelerometer with responses (U, V, W) aligned with their unit vectors $(\hat{u}, \hat{v}, \hat{w})$ and having angles between them ($\varphi_{uv}, \varphi_{vw}, \varphi_{wu}$) that represent the angles between the (U, V), (V, W), and (W, U) accelerometers, respectively. The accelerometers are nearly orthogonal to each other and each have DC offsets defined as (O_u, O_v, O_w). This orientation approximately aligns the axes of maximum responsivity of the U and W accelerometers with the x and y axes of the measurement instrument, respectively.
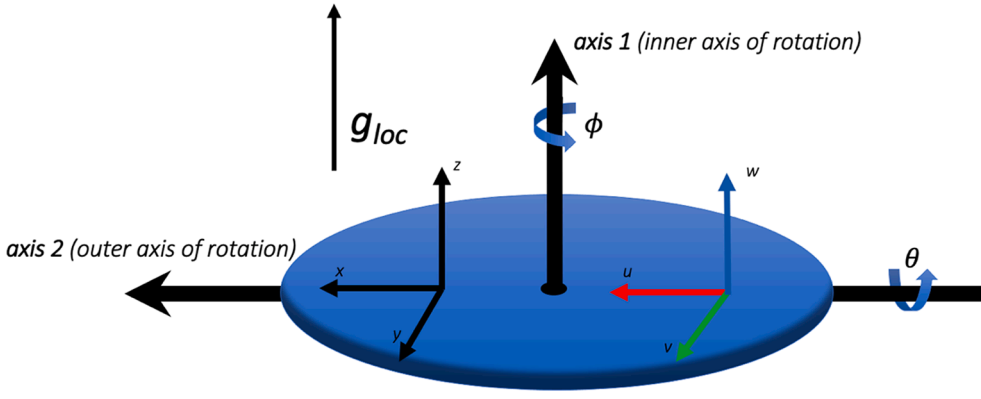
Fig. 2. Depiction of the 2-axis rotation stage with axes of rotation axis 1 and axis 2 with rotation angles of rotation of ϕ and θ, respectively. The stage is shown in its zero position where $\phi = \theta = 0$. The term g_{loc} represents the magnitude and direction of the earth's local gravitational acceleration. The instrument is set up in the laboratory so that the outer axis of rotation, **axis 2**, is always perpendicular to the direction of the gravitational field and the inner axis of rotation, **axis 1**, is parallel to it when $\theta = 0$. The platter of the instrument is defined to have a Cartesian coordinate system as depicted in which the Z axis is always parallel to **axis 1** and the X axis is parallel to **axis 2** when $\phi = 0$. The accelerometer is secured onto the platter so that its (U, V, W) accelerometers are approximately aligned to the (X, Y, Z) coordinate system of the platter.

The protocol to determine the intrinsic properties of the DUT under constant rotation conditions is similar to the orientations used in the static method reported in [12] but instead of stepping the rotation angle in discrete steps the DUT is rotated at a constant angular frequency ω as depicted in Fig. 3.

For the first constant rotation (a), the response of the DUT takes the form:

$$\begin{bmatrix} U^x(t) \\ V^x(t) \\ W^x(t) \end{bmatrix} = \begin{bmatrix} 0 & A^x_{uy}\sin(\omega t) & B^x_{uz}\cos(\omega t) \\ 0 & A^x_{vy}\sin(\omega t) & B^x_{vz}\cos(\omega t) \\ 0 & A^x_{wy}\sin(\omega t) & B^x_{wz}\cos(\omega t) \end{bmatrix} \begin{bmatrix} 1 \\ 1 \\ 1 \end{bmatrix} + \begin{bmatrix} C^x_u \\ C^x_v \\ C^x_w \end{bmatrix}, \qquad (2)$$

where the superscript x denotes the rotation condition (a) around the X axis, the subscripts (u, v, w) denote the response components of the (U, V, W) accelerometers, respectively, and the subscripts (y, z) denote their Y and Z components. The constants (C^x_u, C^x_v, C^x_w) correspond to the device's DC offsets plus a constant centripetal acceleration component for the (U, V, W) accelerometers, respectively.

Similarly, for the second constant rotation condition (b), the response of the DUT takes the form:

$$\begin{bmatrix} U^y(t) \\ V^y(t) \\ W^y(t) \end{bmatrix} = \begin{bmatrix} A^y_{ux}\sin(\omega t) & 0 & B^y_{uz}\cos(\omega t) \\ A^y_{vx}\sin(\omega t) & 0 & B^y_{vz}\cos(\omega t) \\ A^y_{wx}\sin(\omega t) & 0 & B^y_{wz}\cos(\omega t) \end{bmatrix} \begin{bmatrix} 1 \\ 1 \\ 1 \end{bmatrix} + \begin{bmatrix} C^y_u \\ C^y_v \\ C^y_w \end{bmatrix}, \qquad (3)$$

and for the third constant rotation condition (c), the response of the DUT takes the form:

$$\begin{bmatrix} U^z(t) \\ V^z(t) \\ W^z(t) \end{bmatrix} = \begin{bmatrix} A^z_{ux}\sin(\omega t) & B^z_{uy}\cos(\omega t) & 0 \\ A^z_{vx}\sin(\omega t) & B^z_{vy}\cos(\omega t) & 0 \\ A^z_{wx}\sin(\omega t) & B^z_{wy}\cos(\omega t) & 0 \end{bmatrix} \begin{bmatrix} 1 \\ 1 \\ 1 \end{bmatrix} + \begin{bmatrix} C^z_u \\ C^z_v \\ C^z_w \end{bmatrix}. \qquad (4)$$

Each of the three rotation conditions will result in a time series of measurements for the (U, V, W) accelerometers which can be sine fitted using the known value for the constant angular frequency ω to yield the values for each of the A and B coefficients in Eqs. (2)–(4). The C constants are also determined but not used in the further analysis.

To determine the intrinsic sensitivities, we note that the magnitude of the accelerometer responses is related to the square root of the sum of the squares of the A and B coefficients. For the first constant rotation condition (a) we find that the magnitude of the time varying components are related to the sensitivity matrix through Eqs. (2)–(4) as,

$$\begin{bmatrix} (U^x)^2 \\ (V^x)^2 \\ (W^x)^2 \end{bmatrix} = \begin{bmatrix} \left(A^x_{uy}\right)^2 + \left(B^x_{uz}\right)^2 \\ \left(A^x_{vy}\right)^2 + \left(B^x_{vz}\right)^2 \\ \left(A^x_{wy}\right)^2 + \left(B^x_{wz}\right)^2 \end{bmatrix} = (g_{loc})^2 \begin{bmatrix} (s_{uy})^2 + (s_{uz})^2 \\ (s_{vy})^2 + (s_{vz})^2 \\ (s_{wy})^2 + (s_{wz})^2 \end{bmatrix}, \qquad (5)$$

and similarly for constant rotation conditions (b) and (c) we find,

(a) axis 1: 0°
    axis 2: $\omega = 2\pi f$

(b) axis 1: -90°
    axis 2: $\omega = 2\pi f$

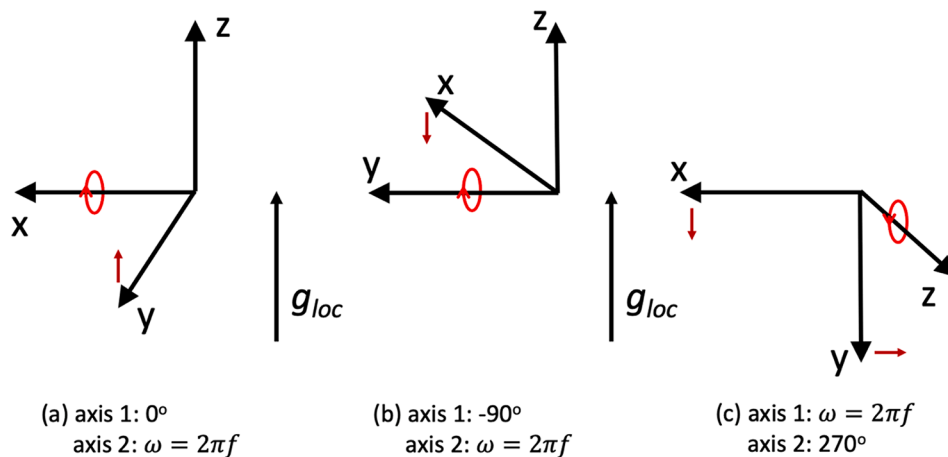(c) axis 1: $\omega = 2\pi f$
    axis 2: 270°

Fig. 3. The three constant rotation conditions for this calibration protocol: (a) rotation around the X axis, (b) rotation around the Y axis, and (c) rotation around the Z axis. All three rotations follow a right-hand rule and are at the same angular frequency $\omega = 2\pi f$, where f is the rotation rate in Hz.

$$\begin{bmatrix} (U^y)^2 \\ (V^y)^2 \\ (W^y)^2 \end{bmatrix} = \begin{bmatrix} \left(A_{ux}^y\right)^2 + \left(B_{uz}^y\right)^2 \\ \left(A_{vx}^y\right)^2 + \left(B_{vz}^y\right)^2 \\ \left(A_{wx}^y\right)^2 + \left(B_{wz}^y\right)^2 \end{bmatrix} = (g_{loc})^2 \begin{bmatrix} (s_{ux})^2 + (s_{uz})^2 \\ (s_{vx})^2 + (s_{vz})^2 \\ (s_{wx})^2 + (s_{wz})^2 \end{bmatrix}, \tag{6}$$

and,

$$\begin{bmatrix} (U^z)^2 \\ (V^z)^2 \\ (W^z)^2 \end{bmatrix} = \begin{bmatrix} \left(A_{ux}^z\right)^2 + \left(B_{uy}^z\right)^2 \\ \left(A_{vx}^z\right)^2 + \left(B_{vy}^z\right)^2 \\ \left(A_{wx}^z\right)^2 + \left(B_{wy}^z\right)^2 \end{bmatrix} = (g_{loc})^2 \begin{bmatrix} (s_{ux})^2 + (s_{uy})^2 \\ (s_{vx})^2 + (s_{vy})^2 \\ (s_{wx})^2 + (s_{wy})^2 \end{bmatrix}. \tag{7}$$

Eqs. (5)–(7) can now be solved to determine the intrinsic sensitivities to yield,

$$s_u = \sqrt{s_{ux}^2 + s_{uy}^2 + s_{uz}^2}$$
$$= \frac{1}{g_{loc}} \sqrt{\frac{\left(A_{ux}^y\right)^2 + \left(A_{ux}^z\right)^2 + \left(A_{uy}^x\right)^2 + \left(B_{uy}^z\right)^2 + \left(B_{uz}^x\right)^2 + \left(B_{uz}^y\right)^2}{2}}, \tag{8}$$

$$s_y = \sqrt{s_{vx}^2 + s_{vy}^2 + s_{vz}^2}$$
$$= \frac{1}{g_{loc}} \sqrt{\frac{\left(A_{vx}^y\right)^2 + \left(A_{vx}^z\right)^2 + \left(A_{vy}^x\right)^2 + \left(B_{vy}^z\right)^2 + \left(B_{vz}^x\right)^2 + \left(B_{vz}^y\right)^2}{2}}, \tag{9}$$

$$s_z = \sqrt{s_{wx}^2 + s_{wy}^2 + s_{wz}^2}$$
$$= \frac{1}{g_{loc}} \sqrt{\frac{\left(A_{wx}^y\right)^2 + \left(A_{wx}^z\right)^2 + \left(A_{wy}^x\right)^2 + \left(B_{wy}^z\right)^2 + \left(B_{wz}^x\right)^2 + \left(B_{wz}^y\right)^2}{2}}. \tag{10}$$

The intrinsic angles $(\varphi_{uv}, \varphi_{vw}, \varphi_{wu})$ are determined from the phase differences by selecting the two larger measured signals (and not using the smaller signal of the three) for each of the rotation conditions. The A and B coefficients are used to determine the phase of each of the signals to express them in the form of $\sin(\omega t + \varphi)$. For example, using the coefficients for the V and W accelerometers from the first constant rotation condition (a) and the corresponding equation (2) the intrinsic angle φ_{vw}, can be determined by phase difference between the V and W waveforms starting with,

$$V^x(t) = A_{vy}^x \sin(\omega t) + B_{vz}^x \cos(\omega t) = \sqrt{\left(A_{vy}^x\right)^2 + \left(B_{vz}^x\right)^2} \cdot \sin(\omega t + \varphi_v^x), \tag{11}$$

and determining the phase shift of the V accelerometer φ_v^x in degrees by,

$$\varphi_v^x = \frac{180}{\pi} \operatorname{atan}\left(\frac{B_{vz}^x}{A_{vy}^x}\right). \tag{12}$$

Similarly, the phase shift for the W accelerometer φ_w^x in degrees is

determined by,

$$\varphi_w^x = \frac{180}{\pi} \operatorname{atan}\left(\frac{B_{wz}^x}{A_{wy}^x}\right). \tag{13}$$

The phase shift of the U accelerometer φ_u^x from the first constant rotation (a) condition is not used in this analysis because it is a relatively small signal compared to the other two. Taking the difference between Eqs. (12) and (13) results in the intrinsic angle φ_{vw},

$$\varphi_{vw} = \varphi_w^x - \varphi_v^x = \frac{180}{\pi} \left[\operatorname{atan}\left(\frac{B_{wz}^x}{A_{wy}^x}\right) - \operatorname{atan}\left(\frac{B_{vz}^x}{A_{vy}^x}\right) \right]. \tag{14}$$

The other two intrinsic angles are determined using the constant rotation conditions (b) and (c) represented by Eqs. (3) and (4), respectively, and following same analysis,

$$\varphi_{wu} = \varphi_u^y - \varphi_w^y = \frac{180}{\pi} \left[\operatorname{atan}\left(\frac{B_{uz}^y}{A_{ux}^y}\right) - \operatorname{atan}\left(\frac{B_{wz}^y}{A_{wx}^y}\right) \right], \tag{15}$$

$$\varphi_{uv} = \varphi_v^z - \varphi_u^z = \frac{180}{\pi} \left[\operatorname{atan}\left(\frac{B_{vy}^z}{A_{vx}^z}\right) - \operatorname{atan}\left(\frac{B_{uy}^z}{A_{ux}^z}\right) \right], \tag{16}$$

It should be noted that using the $\operatorname{atan}()$ function can result in a 180° phase shift in the calculated phase angles. In our analysis we compare the fit with the measured signal by using the calculated phase angle with its functional form, $\sin(\omega t + \varphi)$, by plotting it with the measured signal to ensure their agreement and thereby resolving possible inconsistencies of the phase difference between the signals.

3. Uncertainty analysis

The uncertainty analysis presented here is for the component related to the results of sine fitting to the measurement data. This component primarily addresses the uncertainty due to noise in the measurement but can also include the effects due to nonlinearities in the device response to accelerations. Least squares sine fitting using a fitting function such as LINEST in Microsoft Excel will yield standard error values for the fitting coefficients that can in turn be used to estimate the uncertainties. In this work we are fitting to a function of the form,

$$f(t_i) = A\sin(\omega t_i) + B\cos(\omega t_i) + C, \tag{17}$$

where $f(t_i)$ represents a time series of measurements taken at time $t_i = [t_0, t_1, \ldots t_n]$ and ω is the angular rotation rate of the instrument. The fitting will yield the coefficients A, B, C and their standard errors $SE\{A\}$, $SE\{B\}$, and $SE\{C\}$, respectively. Using equation (8) for the U accelerometer's intrinsic sensitivity, its uncertainty is expressed following a similar procedure presented in [8] using the values of the standard errors as,

$$SE\{s_u\} = \frac{1}{g_{loc}} \sqrt{\frac{\left(A_{ux}^y SE\{A_{ux}^y\}\right)^2 + \left(A_{ux}^z SE\{A_{ux}^z\}\right)^2 + \left(A_{uy}^x SE\{A_{uy}^x\}\right)^2 + \left(B_{uy}^z SE\{B_{uy}^z\}\right)^2 + \left(B_{uz}^x SE\{B_{uz}^x\}\right)^2 + \left(B_{uz}^y SE\{B_{uz}^y\}\right)^2}{2s_u^2}}, \tag{18}$$

and similarly, the uncertainties for the V and W accelerometer sensitivities are expressed as,

where,

$$\frac{d\text{atan}(x)}{dx} = \frac{1}{1+x^2} \quad \frac{\partial x}{\partial A} = -\frac{B}{A^2} \quad \frac{\partial x}{\partial B} = \frac{1}{A} \tag{23}$$

$$SE\{s_v\} = \frac{1}{g_{loc}} \sqrt{\frac{\left(A_{vx}^y SE\{A_{vx}^y\}\right)^2 + \left(A_{vx}^z SE\{A_{vx}^z\}\right)^2 + \left(A_{vy}^x SE\{A_{vy}^x\}\right)^2 + \left(B_{vy}^z SE\{B_{vy}^z\}\right)^2 + \left(B_{vz}^x SE\{B_{vz}^x\}\right)^2 + \left(B_{vz}^y SE\{B_{vz}^y\}\right)^2}{2s_v^2}}, \tag{19}$$

$$SE\{s_w\} = \frac{1}{g_{loc}} \sqrt{\frac{\left(A_{wx}^y SE\{A_{wx}^y\}\right)^2 + \left(A_{wx}^z SE\{A_{wx}^z\}\right)^2 + \left(A_{wy}^x SE\{A_{wy}^x\}\right)^2 + \left(B_{wy}^z SE\{B_{wy}^z\}\right)^2 + \left(B_{wz}^x SE\{B_{wz}^x\}\right)^2 + \left(B_{wz}^y SE\{B_{wz}^y\}\right)^2}{2s_w^2}}. \tag{20}$$

The calculated phase angles for the accelerometers (relative to the arbitrary time t_0 at which sampling is started) are determined in the units of degrees with an equation in the form,

$$\varphi = \frac{180}{\pi} \text{atan}(x), \tag{21}$$

where $x = \left(\frac{B}{A}\right)$. The standard error of this function is expressed by partial derivatives as,

$$SE\{\varphi\} = \frac{180}{\pi} \sqrt{\left(\frac{d\text{atan}(x)}{dx} \frac{\partial x}{\partial A} SE\{A\}\right)^2 + \left(\frac{d\text{atan}(x)}{dx} \frac{\partial x}{\partial B} SE\{B\}\right)^2} \tag{22}$$

and which combined yields,

$$SE\{\varphi\} = \frac{180}{\pi} \frac{\sqrt{(ASE\{B\})^2 + (BSE\{A\})^2}}{A^2 + B^2} \tag{24}$$

Since the intrinsic angles are determined by the difference of the phases of two signals, the standard error contribution from each of the phases is summed in quadrature to find,
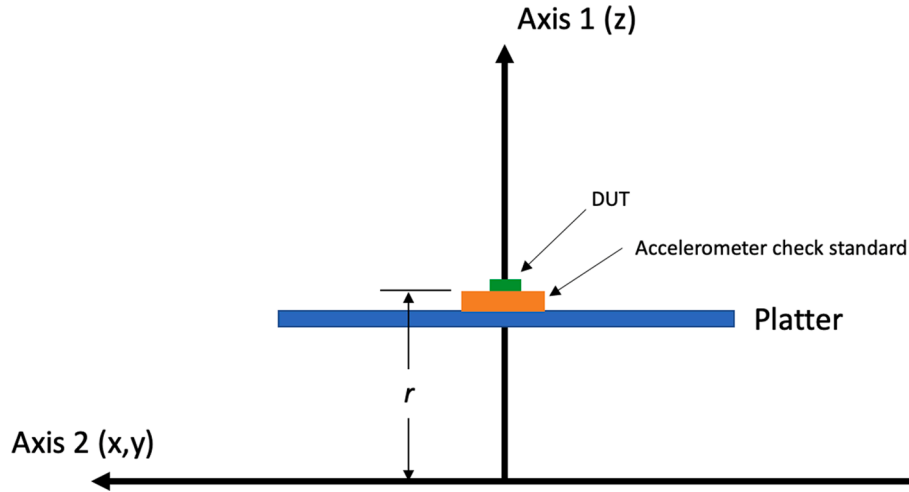

Fig. 4. Diagram of the construction of the instrument depicting the placement of the device under test (DUT) with respect to axis 1 and axis 2 of the instrument. The DUT is displaced by a distance of $r \approx 22$ cm from rotation **axis 2** which corresponds to the distance of the surface of the rotation platter from **axis 2** plus the height of the accelerometer check standard which the DUT is place upon. The x, y axes are perpendicular to **axis 1** and the z axis is parallel to **axis 2**.
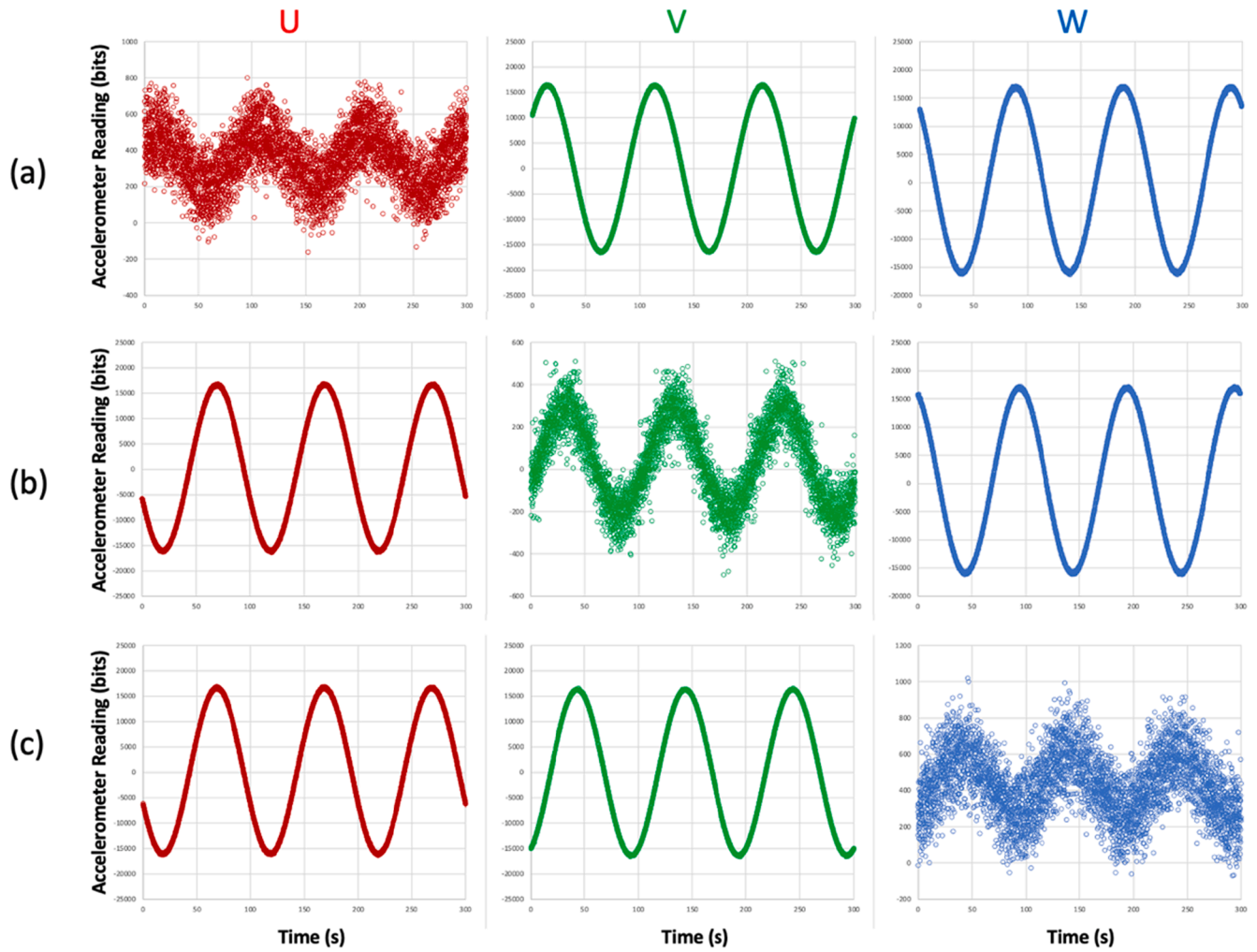
Fig. 5. Data plots of readings from the triaxial digital accelerometer at a rotation rate of 3.6 degrees per second (10 mHz) under the rotation conditions (a) rotation around the x-axis, (b) rotation around the y axis, and (c) rotation around the z axis depicted in Fig. 3. The readings from the U accelerometer are plotted in red, the V accelerometer in green, and the W accelerometer in blue. The accelerometer was read at the maximum data acquisition and communication rate of 16 readings per second. The horizontal axes of the plots are in seconds, ranging from 0 to 300 s, and the vertical axes are in the units of bits, ranging from −25000 to 25,000 bits for the accelerometers that are perpendicular to the axis of rotation and over a reduced range for the accelerometers parallel to the axis of rotation. There are over 4700 data points measured for each of the plots. (For interpretation of the references to colour in this figure legend, the reader is referred to the web version of this article.)

$$SE\{\varphi_{uv}\} = \sqrt{\left(SE\{\varphi_v^z\}\right)^2 + \left(SE\{\varphi_u^z\}\right)^2} = \frac{180}{\pi}\sqrt{\frac{\left(A_{vx}^z SE\{B_{vy}^z\}\right)^2 + \left(B_{vy}^z SE\{A_{vx}^y\}\right)^2}{\left[\left(A_{vx}^z\right)^2 + \left(B_{vy}^z\right)^2\right]^2} + \frac{\left(A_{ux}^z SE\{B_{uy}^z\}\right)^2 + \left(B_{uy}^z SE\{A_{ux}^z\}\right)^2}{\left[\left(A_{ux}^z\right)^2 + \left(B_{uy}^z\right)^2\right]^2}}, \tag{25}$$

$$SE\{\varphi_{vw}\} = \sqrt{\left(SE\{\varphi_v^x\}\right)^2 + \left(SE\{\varphi_w^x\}\right)^2} = \frac{180}{\pi}\sqrt{\frac{\left(A_{vy}^x SE\{B_{vz}^x\}\right)^2 + \left(B_{vz}^x SE\{A_{vy}^x\}\right)^2}{\left[\left(A_{vy}^x\right)^2 + \left(B_{vz}^x\right)^2\right]^2} + \frac{\left(A_{wy}^x SE\{B_{wz}^x\}\right)^2 + \left(B_{wz}^x SE\{A_{wy}^x\}\right)^2}{\left[\left(A_{wy}^x\right)^2 + \left(B_{wz}^x\right)^2\right]^2}}, \tag{26}$$

$$SE\{\varphi_{wu}\} = \sqrt{\left(SE\{\varphi_w^y\}\right)^2 + \left(SE\{\varphi_u^y\}\right)^2} = \frac{180}{\pi}\sqrt{\frac{\left(A_{wx}^y SE\{B_{wz}^y\}\right)^2 + \left(B_{wz}^y SE\{A_{wx}^y\}\right)^2}{\left[\left(A_{wx}^y\right)^2 + \left(B_{wz}^y\right)^2\right]^2} + \frac{\left(A_{ux}^y SE\{B_{uz}^y\}\right)^2 + \left(B_{uz}^y SE\{A_{ux}^y\}\right)^2}{\left[\left(A_{ux}^y\right)^2 + \left(B_{uz}^y\right)^2\right]^2}}. \tag{27}$$

Table 1
Values for the device's intrinsic properties determined by the static method (DC) following the analysis reported in [12] compared to the values determined by the constant rotation method at 10 mHz.

Intrinsic Property	Intrinsic Properties at DC		Intrinsic Properties at 10 mHz Rotation		
	Value	Uncertainty	Value	Uncertainty	Units
U	1669.32	0.41	1669.54	0.66	bits/(m s^{-2})
V	1669.10	0.32	1669.14	0.47	bits/(m s^{-2})
W	1676.46	0.20	1676.43	0.75	bits/(m s^{-2})
φ_{uv}	90.077	0.013	90.099	0.032	°
φ_{vw}	90.095	0.010	90.122	0.034	°
φ_{wu}	89.910	0.012	89.910	0.040	°
O_u	525.1	151.6	–	–	bits
O_v	99.6	29.2	–	–	bits
O_w	442.4	127.8	–	–	bits

4. Experiment

In this report we used a MEMS-based digital triaxial accelerometer [14] as the DUT. It has a nominally flat frequency response from zero to 400 Hz. Therefore, we consider the frequency dependent phase shift of the accelerometers relative to sub-Hz sinusoidal excitation to be negligible.

The DUT was co-integrated with an Arduino microcontroller [15] for the calibration experiment [16]. The microcontroller was programmed to read the digital data from the accelerometers, convert the unsigned binary numbers to decimal numbers, and communicate the readings with a timestamp by Bluetooth wireless communication to the host computer that tabulated the readings in an ASCII data file. The data file was imported into Microsoft Excel for the analysis and to plot the results.

The constant rotation excitation was implemented using a commercially available model AC216-CR 2-Axis Position and Rate Rotation Table manufactured by Acutronic which has a rotation rate range of ±200 °/s on **axis 2** (outer axis) with an accuracy reported by the manufacturer of 0.008 °/s. We used a wireless communication because wired communication by USB through the slip rings of the rotation stage could not be established reliably.

Fig. 4 is a diagram of the construction of the rotation stage which depicts the placement of the device under test (DUT) with respect to **axis 1** and **axis 2** of the rotation stage. The DUT is placed on top of an enclosed triaxial accelerometer that is aligned to the center of the platter that is used as a check standard for our calibrations. The displacement of the DUT from **axis 2** is a combination of the distance of the rotation platter from **axis 2** and the height of the check standard, producing a total displacement of approximately 22 cm. While the U and V accelerometers are aligned close to the center of rotation of **axis 1**, because of the displacement of the DUT from **axis 2** the W accelerometer could see a significant centripetal acceleration as a function of the rotation rate described by the equation $a_c = r\omega^2$, where a_c is the centripetal acceleration, r is the displacement from **axis 2**, and ω is the rotation rate in radians. For example, at a rotation rate of 0.5 Hz with a displacement of 22 cm the centripetal acceleration is calculated to be 2.17 m s^{-2}, which corresponds to 22% of the maximum excitation due to the gravitational acceleration. The centripetal acceleration is a constant which will only contribute to the measurement as an additive effect to the DC offset of the accelerometer. Therefore, in the absence of nonlinearity it would not be expected to contribute to the DUT's sinusoidal response for the calibration under constant rotation as long as the combined effect does not exceed the maximum acceleration of the accelerometer.

The procedure that we used to further characterize the performance of the rotation stage is lengthy and will be reported in a publication to follow but the specifications described here are adequate to support the experimental observations.
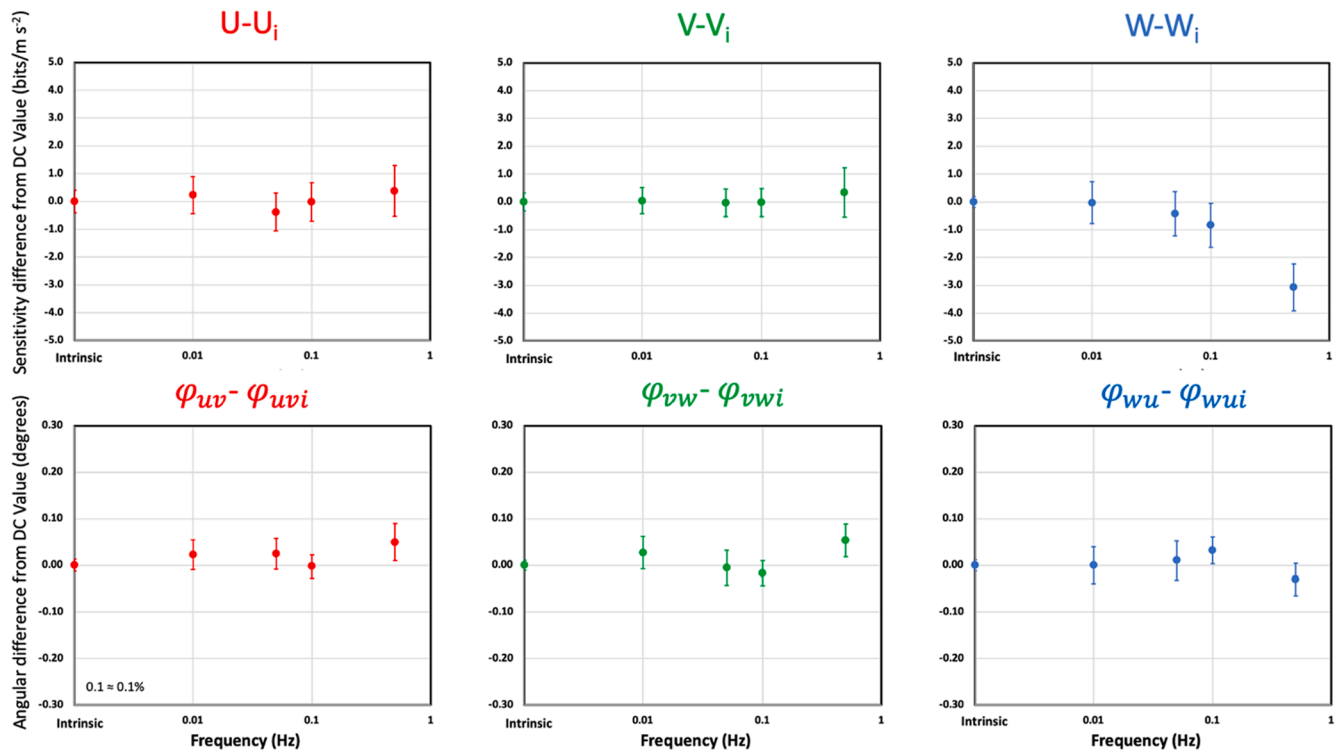

Fig. 6. The device's intrinsic properties measured at 10 mHz, 50 mHz, 100 mHz, and 500 mHz and compared with respect to the static (DC) method reported in [12]. The data is presented as the difference between it and the value determined using the static (DC) method, signified by the subscript i in the plot headings, and plotted together with their uncertainties. These results show that to within their uncertainties the measurements are in agreement for frequencies at and below 0.1 Hz.
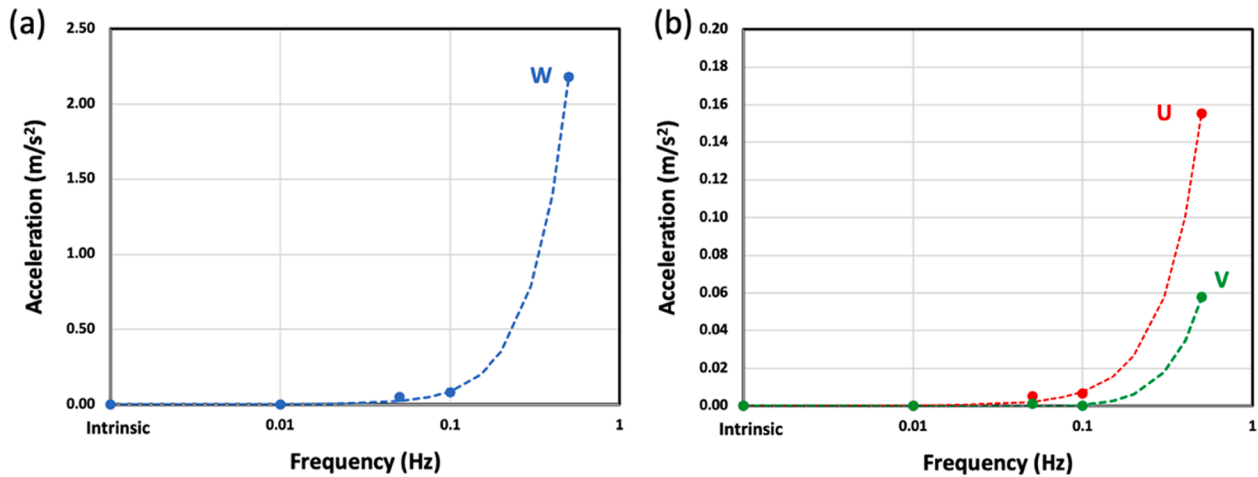
Fig. 7. Plots of the centripetal acceleration calculated from the change in the offset of the accelerometers divided by their calibration factors as a function of the rotation frequency and fitted to a second order polynomial. Plot (a) is for the W accelerometer which has the largest displacement from its axis of rotation, **axis 2**. Plot (b) is for the U and V accelerometers which have a much smaller displacement from their axis of rotation, **axis 1**. The W accelerometer exhibits a more significant effect at 0.5 Hz rotation rate resulting in a substantial value with respect to the local gravitational acceleration.

4.1. Calibration results at 10 mHz rotation rate

Fig. 5 plots the measurement results for the triaxial accelerometer rotated at 10 mHz (3.6 °/s) under the three rotation conditions depicted in Fig. 3, (a) rotation around the x-axis, (b) rotation around the y-axis, and (c) rotation around the (z) axis. The data were analyzed with Microsoft Excel using the analysis presented in Sections 2 and 3 to determine the values for the device's intrinsic properties and measurement uncertainties. These results are tabulated and compared with the static (DC) method reported in [12] in Table 1.

4.2. Comparison of calibration results at 10 mHz, 50 mHz, 100 mHz, 500 mHz rotation rates

Fig. 6 plots a comparison of the device's intrinsic properties calibration at rotation frequencies 10 mHz, 50 mHz, 100 mHz, and 500 mHz with respect to the intrinsic properties measured in static (DC) condition. It is interesting to note that the calculated uncertainties remain approximately constant when an equal number of samples are taken for each of the measurement frequencies. In this experiment 4200 samples were taken at a sampling time interval of 60 ms at each frequency. This is in contrast to measurements based on low frequency vibration where the signal to noise level from the DUT generally decreases with decreasing frequency due to the limitation of the displacement distance, and therefore the maximum acceleration on the vibration exciter, which results in uncertainties that increase with decreasing frequency.

The results show excellent agreement for excitation frequencies of 100 mHz and below but an unexpected deviation is observed at the 0.5 Hz excitation frequency. It is not clear to us whether the deviation is attributable to the actual frequency characteristics of the device or if it is an effect of the centripetal acceleration on the device which is significant compared to gravitational acceleration at that frequency. For example, Prato et. al. reported a similar frequency characteristic, albeit over a higher range of frequencies, for a similar accelerometer. Fig. 7 plots the calculated centripetal acceleration of the accelerometers determined by the change of their offset, referred to as the parameter *C* in Eqs. (2)–(4), divided by their calibration factors. The W accelerometer sees a more significant centripetal acceleration of 22% of the earth's local gravitational acceleration at 0.5 Hz, while the U and V accelerometers exhibit a maximum centripetal acceleration of less than 0.3%. Future work will determine whether this result represents a statistically rare event or shows that the nonlinearity of the W accelerometer is substantially greater than that of the U and V accelerometers. This is plausible

because the U and V accelerometers vibrate parallel to the surface of the MEM die whereas the W accelerometer has a different structure that vibrates perpendicular to the die surface.

5. Conclusions

We have shown that the intrinsic properties of a triaxial accelerometer, consisting of its intrinsic sensitivities and intrinsic angles, can be determined using constant rotation in the earth's gravitational field. The method requires three constant rotation conditions: (a) rotation around the x axis, (b) rotation around the y axis, and (c) rotation around the z axis. The method does not determine the DC offsets of the accelerometers, but those values can be determined from the static (DC) method that we reported previously. The results using the constant rotation method were compared to the static (DC) method and shown to be in agreement to within their calculated uncertainties for frequencies of 10 mHz and less but exhibited a deviation at 0.5 Hz. This suggests that a rotation stage design where the DUT can be placed at the center of the rotation axes could produce an improvement in the method. The results also suggest that a tradeoff can be considered for using this method for very low frequencies versus a vibration calibration method whose uncertainties increase with decreasing frequency below a frequency of minimum uncertainty.

CRediT authorship contribution statement

Michael Gaitan: Conceptualization, Methodology, Software, Investigation, Data curation, Writing – original draft, Writing – review & editing, Visualization. **Jon Geist:** Conceptualization, Methodology, Software, Investigation, Writing – original draft, Writing – review & editing.

Declaration of Competing Interest

The authors declare that they have no known competing financial interests or personal relationships that could have appeared to influence the work reported in this paper.

References

[1] M. Pedley, High-Precision Calibration of a Three-Axis Accelerometer. (2015). Freescale Semiconductor Application Note AN4399, https://www.nxp.com/docs/en/application-note/AN4399.pdf.

[2] The Consultative Committee for Acoustics, Ultrasound and Vibration (CCAUV) is one of 9 committees of the Bureau International ds Poids et Measures (BIPM), https://www.bipm.org/en/committees/cc/ccauv.

[3] H.-J. Martens, Current state and trends of ensuring traceability for vibration and shock measurements, Metrologia 36 (4) (1999) 357–373, https://doi.org/10.1088/0026-1394/36/4/16.

[4] Strategy 2019 to 2029 Consultative Committee for Acoustics, Ultrasound, and Vibration (CCAUV), https://www.bipm.org/utils/en/pdf/CCAUV-strategy-document.pdf.

[5] CCAUV Strategy 2019 to 2029 Summary https://www.bipm.org/utils/en/pdf/CCAUV-strategy-summary.pdf.

[6] A. Umeda, M. Onoe, K. Sakata, T. Fukushia, K. Kanari, H. Iioka, T. Kobayashi, Calibration of three-axis accelerometers using a three-dimensional vibration generator and three laser interferometers, Sens. Actuator A Phys. 114 (1) (2004) 93–101, https://doi.org/10.1016/j.sna.2004.03.011.

[7] G. D'Emilia, A. Gaspari, E. Natale, Calibration test bench for three-axis accelerometers: An accurate and low-cost proposal, in: 2018 IEEE International Instrumentation and Measurement Technology Conference (I2MTC), 2018, https://doi.org/10.1109/I2MTC.2018.8409584.

[8] G. D'Emilia, A. Gaspari, F. Mazzoleni, E. Natale, A. Schiavi, Calibration of tri-axial MEMS accelerometers in the low-frequency range - Part 1: comparison among methods, JSSS 7 (2018), https://doi.org/10.5194/jsss-7-245-2018.

[9] A. Prato, F. Mazzoleni, A. Schiavi, Traceability of digital 3-axis MEMS accelerometer: simultaneous determination of main and transverse sensitivities in the frequency domain, Metrologia 57 (3) (2020) 035013, https://doi.org/10.1088/1681-7575/ab79be.

[10] A. Schiavi, A. Prato, F. Mazzoleni, G. D'Emilia, A. Gaspari, E. Natale, Calibration of digital 3-axis MEMS accelerometers: A double-blind «multi-bilateral» comparison.

[11] J. Geist, M.Y. Afridi, C.D. McGray, M. Gaitan, Gravity-Based Characterization of Three-Axis Accelerometers in Terms of Intrinsic Accelerometer Parameters, J. Res. Natl. Inst. Stan. 122 (32) (2017), https://doi.org/10.6028/jres.122.032.

[12] M. Gaitan, I.M. López Bautista, J. Geist, Reduction of calibration uncertainty due to mounting of 3-axis accelerometers using the intrinsic properties model, Metrologia (2021), https://doi.org/10.1088/1681-7575/abeccf (in press).

[13] The National Geodetic Survey's Surface Gravity Prediction https://www.ngs.noaa.gov/cgi-bin/grav_pdx.prl.

[14] ST Microelectronics LSM6DS33 6DoF inertial measurement unit (IMU) https://www.st.com/en/mems-and-sensors/lsm6ds33.html.

[15] Adafruit Feather nRF52840 Sense https://www.adafruit.com/product/4516.

[16] Certain commercial equipment, instruments, and software are identified in this article in order to describe the experimental procedure adequately. Such identification is not intended to imply recommendation or endorsement by the National Institute of Standards and Technology, nor is it intended to imply that the materials or equipment identified are necessarily the best available for the purpose.

Michael Gaitan Ph.D., is an Engineer Emeritus in the Quantum Measurement Division at NIST.

Jon Geist Jon Geist, Ph.D., is an Electrical Engineer in the Quantum Measurement Division at NIST.

The National Institute of Standards and Technology is an agency of the U.S. Department of Commerce.